3D Hyaluronic Acid Hydrogels for Modeling Oligodendrocyte Progenitor Cell Behavior as a Function of Matrix Stiffness

Deniz B. Unal[1], Steven R. Caliari[1,2*], Kyle J. Lampe[1*]

[1]Department of Chemical Engineering, [2]Department of Biomedical Engineering, University of Virginia, Charlottesville, Virginia 22903, United States

[*]Co-corresponding authors

Keywords:

Oligodendrocyte progenitor cell, hyaluronic acid, tissue engineering, central nervous system

Abstract:

The lack of regenerative solutions for demyelination within the central nervous system (CNS) motivates the development of strategies to expand and drive the bioactivity of the cells, including oligodendrocyte progenitor cells (OPCs), that ultimately give rise to myelination. In this work, we introduce a 3D hyaluronic acid (HA) hydrogel system to study the effects of microenvironmental mechanical properties on the behavior of OPCs. We tuned the stiffness of the hydrogels to match brain tissue (storage modulus 200 – 2000 Pa) and studied the effects of stiffness on metabolic activity, proliferation, and cell morphology of OPCs over a 7 day period. Although hydrogel mesh size decreased with increasing stiffness, all hydrogel groups facilitated OPC proliferation and mitochondrial metabolic activity to similar degrees. However, OPCs in the two lower stiffness hydrogel groups (170 ± 42 Pa and 794 ± 203 Pa) supported greater adenosine

triphosphate (ATP) levels per cell than the highest stiffness hydrogels (2179 ± 127 Pa). Lower stiffness hydrogels also supported higher levels of cell viability and larger cell spheroid formation compared to the highest stiffness hydrogels. Together, these data suggest that 3D HA hydrogels are a useful platform for studying OPC behavior and that OPC growth/metabolic health may be favored in lower stiffness microenvironments mimicking brain tissue mechanics.

Introduction:

One of the major life-altering effects of central nervous system (CNS) disorders is demyelination, with multiple sclerosis being the most common disease pathology.[1] Without the lipid-based myelin sheath to insulate neuronal axons, these axons that rely on efficient node to node conduction revert to inefficient continuous conduction. In turn, this leads to protease activation, axonal degradation, axonal loss, and ultimately neuronal death.[2] The associated loss of function motivates the development of strategies to promote "remyelination" or the regeneration of the myelin sheath after degeneration. Oligodendrocyte progenitor cells (OPCs) of the CNS are one of the most important cell types in remyelination research.[3] OPCs are distributed through the white matter in the adult brain and differentiate into mature oligodendrocytes.[4] Oligodendrocytes myelinate the axons of neurons in the CNS (counterparts to Schwann cells in the peripheral nervous system) to increase efficiency and precision of electrical impulse conduction.[5] Remyelination after injury may follow similar processes to developmental myelination. OPCs can be recruited and activated in the acute inflammation stage of multiple sclerosis lesion formation[6–9] but rarely in the chronic stages of the disease.[2,10] Controlled exogenous OPC transplantation could be leveraged toward regenerative remyelination as OPCs have been used in pre-clinical[11–15] and clinical trials[16] to drive remyelination in vivo. Together these studies motivate the need to

understand microenvironmental cues supporting sustained OPC viability and bioactivity. The future clinical applications of OPCs will likely require scale up of OPC production, which is more efficient in 3D culture systems.

Hydrogels are useful 3D biomaterials for modeling CNS extracellular environments as they are mechanically compliant, permit biomolecule transport, and facilitate cell behaviors including adhesion, proliferation, and migration.[17–19] OPCs and their precursors (neural stem cells) have been studied in polyethylene glycol (PEG)[20], collagen, agarose, chitosan, and fibrin hydrogels.[21,22] Hyaluronic acid (HA) is an excellent candidate for engineering brain-like extracellular matrix (ECM) microenvironments[23,24] due to its abundance in the CNS[25–27] and its anti-inflammatory role in brain and spinal cord injuries.[28] Gelatin-functionalized HA hydrogels support 2D OPC culture and process extension as well as remyelination of demyelinated axons following implantation in a rat spinal cord injury model.[29] HA hydrogels engineered to match brain tissue stiffness also support neuronal progenitor cells (NPC) viability and neuronal differentiation.[30] The success of HA materials is likely mediated through direct cellular interactions with HA through the expression of CD44, the primary cell surface receptor that binds HA, which is expressed in oligodendroglial lineages.[25] Elevated CD44 expression can also slow OPC maturation, which may be beneficial for preserving OPC progenitor states and enabling the expansion of OPCs in vitro.[31]

Hydrogel cell culture models enable interrogation of the roles that extracellular cues such as matrix stiffness play in regulating salient cell behaviors.[20,32–34] Jagielska et al. showed that OPCs are mechanosensitive, with proliferation being greatest on 2D substrates with Young's elastic moduli of 700 Pa.[35] Similarly, Li et. al. found that proliferation was greatest on 2D HA hydrogels with shear moduli of 116 Pa.[29] 3D culture systems offer the potential to study cell-cell

and cell-matrix interactions as well as biotransport conditions in a more physiologically-relevant setting. We previously showed that OPC metabolic activity was greatest within 3D PEG hydrogels with storage moduli of 240 ± 84 Pa in comparison to 630 ± 79 Pa and stiffer conditions.[36] In this work, we used 3D HA hydrogels to interrogate the effects of stiffness and mesh size on OPC proliferation, metabolic activity, and spheroid volume. By utilizing HA, we aim to compare our previous results to a more physiological, but stiffness-matched, biomaterial environment for OPC culture .[37]

Materials & Methods:

Cell culture:

Green fluorescent protein positive (GFP+) mosaic analysis with double markers (MADM) OPCs were expanded on T75 (Corning CellBind) treated tissue culture plates. MADM cells are derived from mouse glioma cells that express many OPC markers.[36] Used to determine the OPC as the cell of origin of glioma through derivation from NPCs,[38] these MADM cells follow the developmental lineage of OPCs and achieve the same proliferative OPC state in vitro. Tissue-cultured plates were coated with polyornithine (10 μg/mL) and rinsed thrice with Dulbecco's phosphate buffered saline (PBS). OPC proliferation media consisted of Dulbecco's modified Eagle's medium (DMEM, Life Technologies) with 4 mM L-glutamine and 1 mM sodium pyruvate (Life Technologies), N2 supplement (Life Technologies) and B27 supplement (Life Technologies), and 1% penicillin-streptomycin (Life Technologies). Cells were seeded at 0.5 x 10^4 cells/cm^2 in 8 mL of proliferation media. Media was changed every two days. Passaging was performed when cells reached 80% confluence. Cyropreserved cells were passaged at least once before use in hydrogel experiments. Cells from passage numbers 10-25 were used.

NorHA macromer synthesis:

HA-TBA synthesis: Research grade sodium hyaluronate (Lifecore Biomedical, 61.8 kDa) was converted to its tetrabutylammonium (TBA) salt (HA-TBA) to prepare for dissolution in DMSO.[40] Sodium hyaluronate was dissolved in DI water at 2 wt% and Dowex resin (50W x 200) was added at a ratio of 3 g resin/1 g HA.[40] The resin exchanges sodium ions for hydrogen ions, making the solution strongly acidic. The solution was stirred for ~ 2 hrs. Stirring was stopped to allow the resin to settle to the bottom of the flask. The solution was then vacuum filtered until the solution was clear to remove all resin. The solution was titrated to pH 7.02-7.05 with TBA-OH. The HA-TBA solution was then frozen at -80 ºC and lyophilized. Tubes were purged with N_2 and stored at -20 ºC.

NorHA synthesis: In a dried and stoppered round bottom flask, HA-TBA and Nor-amine (5-norbornene-2-methylamine) were added. Nor-amine was added to modify ~ 20-30% of HA disaccharides. Anhydrous DMSO was added via cannulation to the flask (~ 5 mL per 0.1 g). Once the HA-TBA was fully dissolved, benzotriazol-1-yloxytris(dimethylamino)phosphonium hexafluorophosphate (BOP) was added at a 0.3:1 molar ratio of BOP to TBA functional groups on the HA-TBA via cannulation with the BOP dissolved in ~ 20 mL of anhydrous DMSO. The reaction was allowed to proceed for ~ 2 h and then quenched with ~ 10 mL of DI water. The solution was transferred to dialysis tubing (molecular weight cutoff: 6-8 kDa) and put on dialysis for 5 days, the first 3 of which included ~ 5 g of NaCl in ~ 5 gal of DI water to help remove TBA. Through filtration, the side-products from the BOP coupling were removed. The solution was then returned to dialysis for 3-5 days. Finally, the solution was transferred to 50 mL tubes, frozen at -80 ºC, and lyophilized to dry. A representative ^{1}H NMR spectrum can be found in **Figure S1**.

Hydrogel preparation:

Hydrogel precursor solutions were prepared to final concentrations of 1–2 wt% NorHA macromer, 0.0328 wt% lithium phenyl-2,4,6-trimethylbenzoylphosphonate (LAP) photoinitiator, and dithiothreitol (DTT, Sigma-Aldrich) crosslinker at a 0.315:1 ratio of thiol:norbornene in PBS. Solutions were sterilized via germicidal UV irradiation for 2.5 h. OPC MADM cells were combined with the precursor solution and encapsulated in hydrogels at a final concentration of 5 x 10^6 cells/mL using 365 nm UV light (4 mW/cm^2, 2 min).

Oscillatory shear rheology:

Oscillatory shear rheology was used to assess gelation kinetics and hydrogel viscoelastic properties. 50 µL of hydrogel precursor solution was pipetted onto a UV-configured plate of an Anton Paar MCR 302 rheometer. A 25 mm diameter smooth cone and plate with a 0.505º angle was used for all studies. Hydrogels were cured *in situ* at 0.1% oscillatory strain, 10 rad/s oscillation frequency, and 4 mW/cm^2 UV light intensity (365 nm). After 30 s of pure oscillatory motion, light exposure was introduced underneath the plate for 120 s. Time sweep data was recorded for an additional 60 s after light exposure ceased.

Swelling studies:

360 µL hydrogels were fabricated in 3 mL syringes using the formulations and polymerization conditions already described. Samples were then soaked in PBS at 37 ºC. At time points of 0, 24, and 48 h after gelation, samples were weighed after blotting away excess liquid. These samples were then lyophilized and the dry mass was recorded. Two experimental replicates were conducted

with n = 3-4 per sample type per time point. Flory-Rehner calculations[41] were used to determine mass and volumetric swelling ratios (**Table S1**), molecular weight between crosslinks, and mesh size. First the molecular weight between crosslinks was determined through the equilibrium swelling theory for crosslinked polymers[42]:

$$\frac{1}{M_{c,S}} = \frac{2}{M_n} - \frac{v/V_1[\ln(1-v_{2,s})+(v_{2,s})+\chi(v_{2,s})^2]}{(v_{2,r})[\left(\frac{v_{2,s}}{v_{2,r}}\right)^{\frac{1}{3}}-\frac{v_{2,s}}{2v_{2,r}}]} \quad (1)$$

Where $M_{c,S}$ is the molecular weight between crosslinks estimated from swelling (g/mol), M_n is the molecular weight of the macromer (61,800 g/mol), v is the specific volume of the macromer (0.8137 mL/g), V_1 is the molar volume of the solvent (18 mol/cm^3), χ is the polymer solvent interaction parameter, $v_{2,r}$ is the volume fraction of polymer in the relaxed state, and $v_{2,s}$ is the volume fraction of polymer in the swollen state (see supplemental information for more details). The polymer solvent interaction parameter can be taken as 0.473 because of the similarities between the polysaccharides hyaluronic acid and dextran.[41,43] The effective crosslinking density and mesh size calculations are then adapted from Leach et al.[43]

$$v_e = \frac{\rho_p}{M_{c,S}} \quad (2)$$

Where v_e is the effective crosslinking density (mol/cm^3), and ρ_p is the density of the dry polymer (g/mL). This allows calculation of the mesh size using the equation below:

$$\xi = 0.1743(v_{2,s})^{-\frac{1}{3}}(M_{c,S})^{\frac{1}{2}} \quad (3)$$

Where ξ is the mesh size (nm).

Quantification of OPC mitochondrial metabolic activity:

OPC mitochondrial metabolic activity was measured using the AlamarBlue assay. In AlamarBlue, the chemical compound resazurin is reduced to resorufin through cellular respiration. The

metabolic activity is represented by percent reduction and can be measured through absorbance or fluorescence intensity. The Beer-Lambert law is used when measuring absorbance values. Equations 4, 5, and 6 describe the phenomena.

$$\varepsilon_{RED}\lambda_1 C_{RED} + \varepsilon_{OX}\lambda_1 C_{OX} = A\lambda_1 \quad (4)$$

$$\varepsilon_{RED}\lambda_2 C_{RED} + \varepsilon_{OX}\lambda_2 C_{OX} = A\lambda_2 \quad (5)$$

$$C_{RED/C} = \frac{(\varepsilon_{OX}\lambda_2 A\lambda_1) - (\varepsilon_{OX}\lambda_1 A\lambda_2)}{(\varepsilon_{OX}\lambda_2 P\lambda_1) - (\varepsilon_{OX}\lambda_1 P\lambda_2)} \quad (6)$$

Where $\varepsilon\lambda$ is the molar extinction coefficient (oxidized or reduced form) at the excitation or emission wavelength (570 nm = λ_1, 600 nm = λ_2), $A\lambda$ is the absorbance value of the sample at the excitation or emission wavelength, C is the concentration of AlamarBlue (oxidized or reduced form), and $P\lambda$ is the absorbance of the control wells (excitation or emission). AlamarBlue reagent (ThermoFisher) was mixed with OPC proliferation media at a 1:9 ratio as specified by the manufacturer. Each hydrogel with encapsulated cells was incubated in 400 µL of this pre-made solution for 4 h at 37 °C. Hydrogels were then removed from solution and returned to OPC proliferation media for further culture. Remaining solution for each sample was pipetted into three 100 µL replicates along with three 100 µL replicates of blank AlamarBlue/media solution. Absorbance was read in a BMG Clariostar monochromator microplate reader.

Live/Dead assay:

OPC viability in HA hydrogels was measured using the Live/Dead assay. Each hydrogel was suspended in 1 mL of PBS plus glucose (PBSG) with the same concentration of glucose as in OPC proliferation media (25 mM). Live/Dead staining consisted of 4 µM ethidium homodimer (to label dead cells) with incubation at 37 ºC for 60 minutes followed by rinsing 2x with PBSG. Live cells

were visualized using GFP signal from MADM OPCs. Live/Dead images were collected using a Zeiss LSM 510 confocal microscope with ~ 500 µm z-stacks (10 µm slices).

Cell Glo:

OPC ATP activity was measured using the Cell Glo assay. Hydrogel samples were homogenized in 400 uL of lysis buffer (20 mM Tris-HCl, 150 mM NaCl, 1 mM Na_2EDTA, 1 mM EGTA, 1% Triton X-100, 2.5 mM sodium pyrophosphate, 1 mM β-glycerophosphate, 1 mM Na_3VO_4, 1 µg/mL leupeptin). First, a standard curve for ATP was made using the manufacturer's protocol. Cell Glo reagent was prepared by adding 10 mL of CellTiter-Glo buffer to the CellTiter-Glo substrate (CellTiter-Glo, Promega) to reconstitute the lyophilized enzyme mixture. Solution was gently mixed through inversion. Once completely dissolved, the solution was stored at – 20 ºC in 1 mL aliquots. A white 384-well plate was used for the assay. 25 µL of each standard was added with three pipetting replicates. 5 µL of sample was diluted with 20 µL of PBS in each well. To all wells (standards and samples), 25 µL of Cell Glo reagent was added. The plate was incubated at room temperature for 10 minutes and luminescence was measured using a BMG Clariostar microplate reader. A standard curve was plotted relating luminescence values to ATP concentrations. Sample ATP concentrations were then determined based on the standard curve.

Pico Green:

OPC DNA content was measured using the Pico Green assay. Hydrogel samples were homogenized in 400 uL of lysis buffer (20 mM Tris-HCl, 150 mM NaCl, 1 mM Na_2EDTA, 1 mM EGTA, 1% Triton X-100, 2.5 mM sodium pyrophosphate, 1 mM β-glycerophosphate, 1 mM Na_3VO_4, 1 µg/mL leupeptin). First, a standard curve for DNA was made using the manufacturer's

protocol. A black 384-well plate was used for the assay. Standards were pipetted at 20 µL with three pipetting replicates. Samples were pipetted with three pipetting replicates and three sample replicates at 5 µL sample volume and 15 µL 1x TE buffer (10 mM Tris-HCl, 1 mM disodium ethylenediaminetetraacetic acid (EDTA), pH 8.0). 20 µL of 1X Pico Green reagent (Quant-iT, Thermo Fisher Scientific) was added to all the standards and samples. Fluorescence was measured in a BMG Clariostar microplate reader according to the manufacturer's directions. A standard curve was plotted relating fluorescence values to DNA concentrations. Sample DNA concentrations were then determined based on the standard curve.

Spheroid volume measurement:

OPC spheroid volumes were measured using Live/Dead confocal images. Z-stacks of ~ 500–1500 µm thickness (10 µm slices) were loaded in ImageJ. GFP and ethidium homodimer channel images were analyzed separately using the "3D object counter" module in ImageJ. This module performs image thresholding followed by counting and sizing of each spheroid. The volume of each GFP+ spheroid was determined. The average spheroid volume was calculated for each experimental condition and time point. In addition, the average spheroid volume was normalized to the hydrogel volume. The average hydrogel volume occupied by cell spheroids (a fraction of the hydrogel occupied by live cells) was calculated by summing the volume of spheroids within each image stack, normalizing to the hydrogel volume, and then averaging between three hydrogels per experimental condition per time point. A total of 3613–14870 spheroids were measured per experimental condition at a given time point. Three confocal image stacks were taken per sample. Two or three samples were analyzed from each experiment and time point. Five experimental

replicates were performed, yielding 12-15 samples per condition per time point for each hydrogel experimental group.

Statistical analysis:

ATP, DNA, metabolic activity, and spheroid volume data were analyzed using two-way ANOVA followed by the Tukey post-hoc test with α-value of 0.05. Calculations were performed using SPSS software. Box plots cover the second and third data quartiles with error bars covering the first and fourth quartiles. Box plots also include marks for mean (*x*) and median (*bar*) data values.

Results & Discussion:

Mechanical Properties of NorHA Hydrogels

The NorHA hydrogels were formed through the crosslinking of norbornene groups with dithiol crosslinker (DTT) via radical-mediated thiol-ene addition using a LAP photoinitiator that absorbs strongly at 365 nm (**Figure 1**). Norbornene groups preferably crosslink with thiyl radicals instead of with themselves, creating a phototunable hydrogel system where the degree of crosslinking is controlled by the molar ratio of thiol to norbornene groups.[40] Gramlich et al. demonstrated the positive correlation between NorHA hydrogel stiffness and thiol to norbornene crosslinking ratio up to 0.8.[40] We also previously demonstrated the suitability of NorHA hydrogels for 3D cell culture across a range of Young's moduli from ~ 1-15 kPa.[44] In this work, the molar ratio of thiol to norbornene groups was kept constant at 0.315 while the NorHA macromer concentration was varied between 1 and 2 wt% to enable fabrication of hydrogels spanning a range of CNS-relevant stiffnesses.

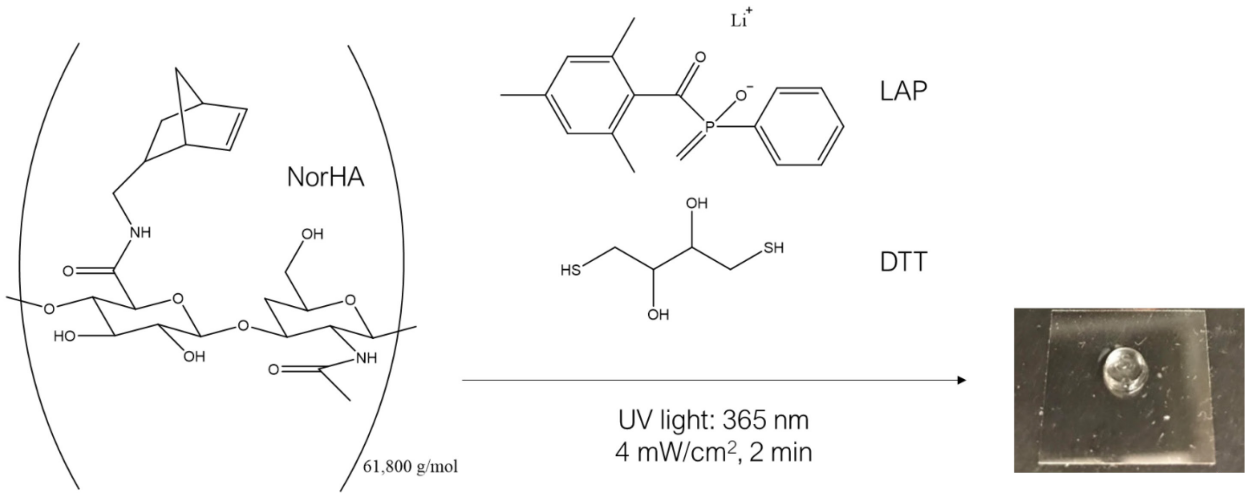

Figure 1: **Schematic of hydrogel formation.** 20-28% of the hyaluronic acid disaccharide repeat units were modified with norbornene functional groups. Norbornenes were crosslinked with dithiol crosslinker (DTT) to form hydrogels. Hydrogels were photocrosslinked under 4 mW/cm^2 (365 nm) light for 2 minutes using LAP as the photoinitiator.

Cells sense mechanical cues and respond to them through mechanotransduction-mediated changes in morphology, metabolic activity, and proliferation.[45] Storage modulus and mesh size are key properties affecting these cell traits.[36] Storage modulus dictates the stiffness of the material while mesh size dictates the spacing between crosslinks and availability for cell colony growth and biomolecule diffusion. Storage modulus can be measured through oscillatory shear rheology (**Figure 2**).

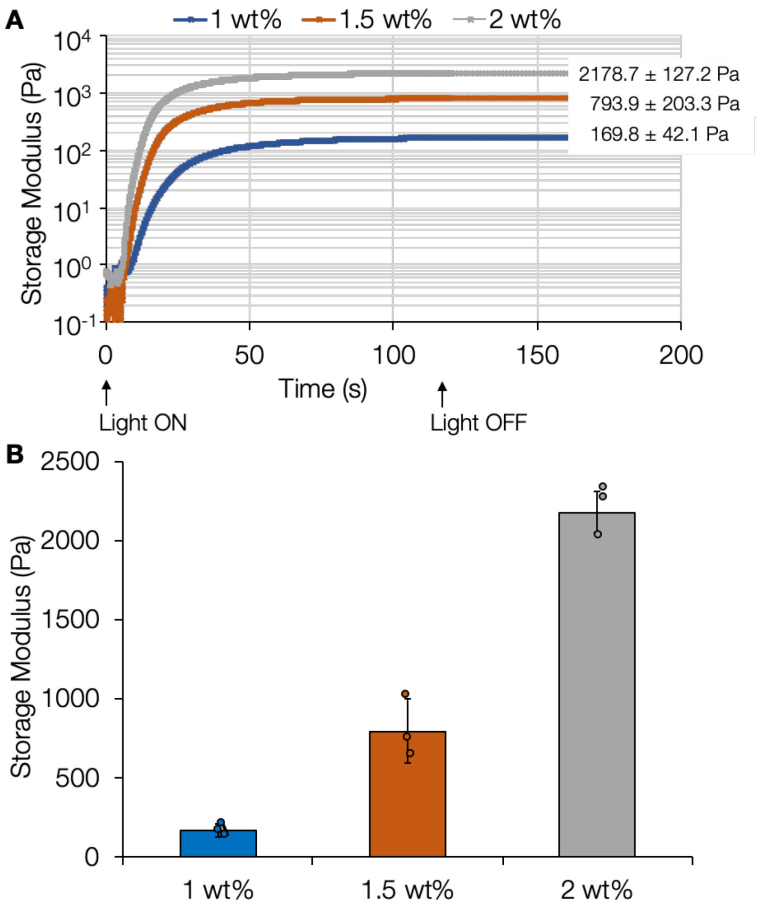

Figure 2: Rheological properties of crosslinked HA hydrogels. (A) Average storage modulus was determined from oscillatory shear rheology time sweeps performed on NorHA hydrogels crosslinked *in situ* at 1 wt% (wt/v), 1.5 wt%, or 2 wt%. Hydrogels were formed by exposure to UV light from 0 to 120 s. (B) Averaged plateau modulus (*bar*) was measured from individual trials (*circles*). Plateau storage modulus was calculated from the average modulus of 150–180 s (30-60 s after the light is turned off) for each trial. Loss moduli (~ 1 Pa) do not significantly change between the experimental groups for these elastic hydrogels. *Error bars*: standard deviation, $n = 3$ hydrogels per experimental group.

Formulations of NorHA hydrogels were adjusted to match the range of brain tissue stiffness (i.e., 200-2000 Pa).[46] 1, 1.5, and 2 wt% formulations corresponding to storage moduli of 170 ± 42 Pa, 794 ± 203 Pa, and 2179 ± 127 Pa, respectively, dictating the elastic behavior. Hydrogels reached swelling equilibrium within 24 hours (**Table S1**). Mesh sizes at equilibrium were determined through Flory-Rehner polymer theory (Materials and Methods). In comparison

to previous studies with PEG-dimethacrylate (PEGDM) hydrogels, the NorHA hydrogels have 6-7 fold larger mesh sizes (**Table 1**) and much greater swelling ratios (**Table S1**), suggesting that the NorHA hydrogels could allow for greater cell growth or process extension while still appropriately mimicking CNS tissue stiffness. In previous work, the degree of methacrylation modification of PEGDM hydrogels was 82-86%[36] while here the degree of modification of NorHA hydrogels was 20-28%. Leach et al. performed swelling studies with hydrogels made from glycidyl methacrylate-HA (GMHA) that was two orders of magnitude greater in molecular weight than the HA used here but only 5-11% functionalized with methacrylate groups.[43] Molecular weight between crosslinks was also found to be two orders of magnitude greater (not reported here) compared to our NorHA hydrogels.[43] Consequently, mesh sizes were an order of magnitude greater than those calculated for our NorHA hydrogels.

Stiffnesses were comparable for NorHA and PEGDM hydrogels. The complex moduli of GMHA hydrogels can be directly compared with the storage moduli for NorHA hydrogels as the loss moduli for NorHA hydrogels are consistently ~ 1 Pa. While stiffness is typically inversely correlated with mesh size, stiffness is not a direct indication of mesh size. The results of our study and others[36,43] show that hydrogel mesh size depends on a combination of the degree of functionalization, the molecular weight of the polymer, and the crosslinking density. Interestingly, these NorHA hydrogels, while exhibiting high swelling ratios, underwent relatively small increases in volume of 10-27% at 24 hours (**Table S1**). This may be advantageous in maintaining a high cell density, and thus maximizing important pericellular signaling.

Work Source	Molecular Weight (g/mol)	Degree of functionalization (%)	Sample Type	Storage Modulus (Pa)	Mesh Size (nm)
Present Study	61,800	20-28	1 wt% NorHA	170 ± 42	86 ± 3
Present Study	61,800	20-28	1.5 wt% NorHA	794 ± 203	76 ± 4
Present Study	61,800	20-28	2 wt% NorHA	2179 ± 127	73 ± 4
Reference 36	8,000	82-86	6 wt% PEGDM	240 ± 84	12.5
Reference 36	6,000	82-86	6 wt% PEGDM	270 ± 87	9
Reference 36	4,600	82-86	6 wt% PEGDM	630 ± 79	8.2
Reference 43	2,000,000	5	1 wt% GMHA	109 ± 16*	644
Reference 43	2,000,000	7	1 wt% GMHA	131 ± 6*	619
Reference 43	2,000,000	11	1 wt% GMHA	155 ± 28*	539

Table 1: Hydrogel mesh sizes. Comparison of NorHA hydrogel mesh sizes with PEGDM hydrogel mesh sizes[36] and GMHA hydrogel mesh sizes[43] (* indicates complex shear modulus). Mesh sizes were calculated from swelling studies measuring equilibrium (swollen) wet mass and lyophilized dry mass to obtain mass / volumetric swelling ratios. $n = 8$ hydrogels per experimental group.

Effects of Hydrogel Mechanical Properties on OPC Morphology, Proliferation, and Metabolic Activity

After synthesizing hydrogels with mechanical properties resembling CNS tissue, we encapsulated OPCs in NorHA hydrogels and assessed their viability through confocal fluorescence microscopy over 7 days of culture. Live/Dead imaging showed that OPCs could remain viable in all hydrogel formulations (**Figure 3**). Since NorHA hydrogels have larger mesh sizes than PEGDM hydrogels, we would also expect OPC spheroid volumes to be larger. Representative max projections of OPCs in hydrogels (**Figure 3**) visually show similar viabilities at day 1, but by day 7, the 1 wt% conditions appears to have the most viable cells. The vast majority of cells in these hydrogels exhibited rounded morphologies, which corroborates previous work showing that OPC process extensions inside 3D hydrogels decrease significantly when the elastic modulus is > 120 Pa.[47]

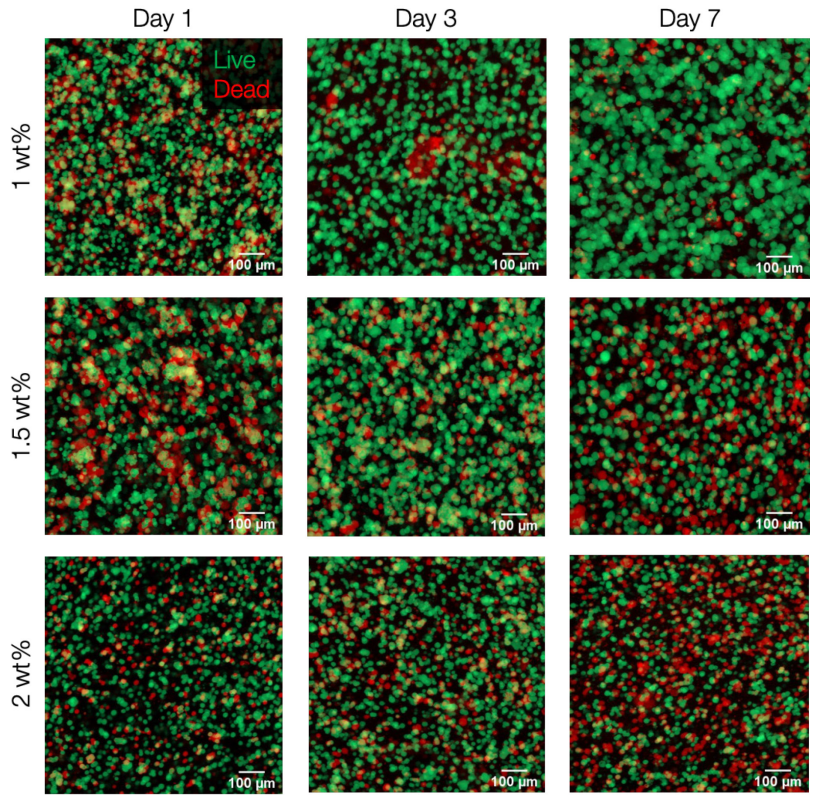

Figure 3: OPC viability in NorHA hydrogels. Standard deviation z-stack projections (770-1930 µm depth) of GFP+ OPCs (live cells, *green*) and ethidium homodimer-labeled dead cells (*red*) in NorHA hydrogels. 1 wt% hydrogels appear to show the largest average spheroid volumes and highest viability after 7 days of culture.

We used confocal live/dead images to measure OPC spheroid size and plotted the distribution of the entire population in **Figure 4**. We previously reported an average OPC spheroid diameter of 21 µm for ~ 600 Pa stiffness and 10 nm mesh size PEGDM hydrogels.[36] In the current study, average OPC spheroid diameters were at least 1.5 fold greater in hydrogels of ~ 795 Pa stiffness and 76 nm mesh size. NorHA hydrogels of ~ 170 Pa and 85 nm mesh size had 2-2.5 fold greater spheroid diameters than the ~ 600 Pa stiffness and 10 nm mesh size PEGDM hydrogels. This is consistent with the concept that larger mesh sizes lead to larger spheroid sizes, especially in hydrogels that are not engineered to degrade via hydrolysis or cell-secreted enzymes. In terms of absolute spheroid size, lower stiffness 1 wt% hydrogels did trend toward supporting the largest

spheroid volumes after a 7 day culture period (**Figure 4)** although not statistically significant differences were observed.

While bioactivity of HA is a complicating factor regarding cell behavior in comparison to non-adhesive PEG,[37] the result of significantly larger spheroid volumes in 1 wt% hydrogels at day 7 in comparsion to 1.5 wt% and 2 wt% on the same day indicate that effects of HA-cell interactions due to CD44 are not stimulative, since 1 wt% experimental group would present the least amount of potential CD44 binding sites. Furthermore, the norbornene modification of HA significantly decreases the CD44 engagement with other cell types[48], and thus differences in CD44 engagement between the hydrogel conditions studied here are unlikely. Thus, the effects of any potential HA-cell engagement is likely minimal in comparison to effects of stiffness and mesh size. Degradation via hydrolysis is minimal as evidenced by a lack of change in mass swelling ratios after 2 days of incubation (table S1). In the presence of cells however, some cell-mediated enzymolysis via hyaluronidase may occur.

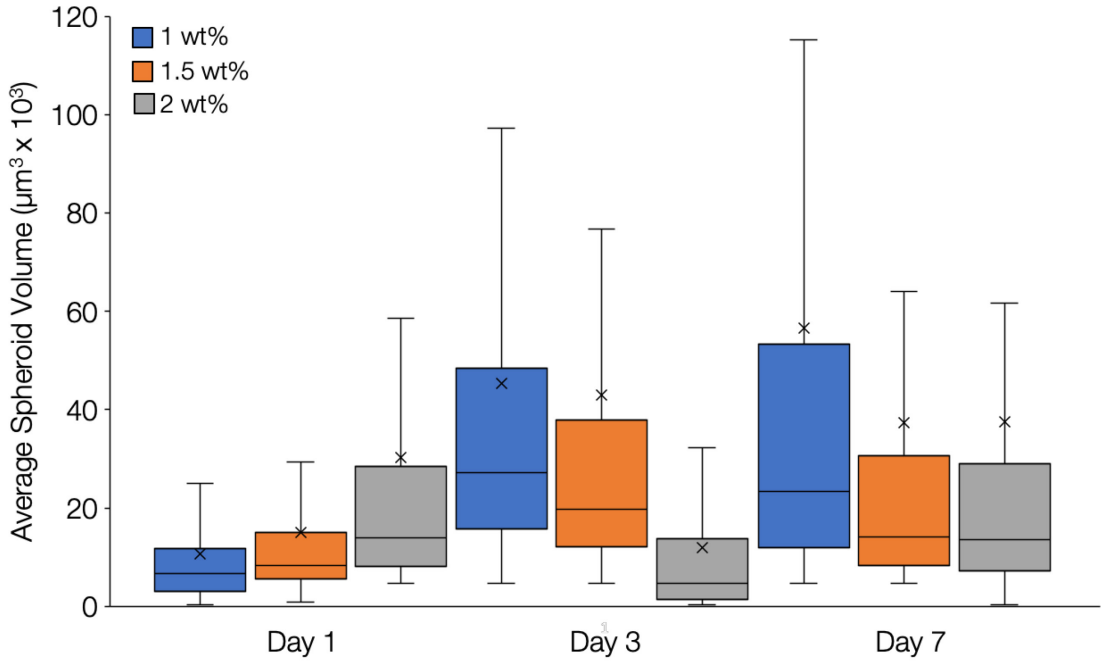

Figure 4: OPC spheroid volume. Average live spheroid volume was determined using the 3D object counter tool in ImageJ. 1 wt% hydrogels supported the largest average spheroid volume after 7 days of culture. Data presented for each group includes the mean (*x*) and median (*bar*). Whiskers represent the 1st and 4th quartiles while boxes represent the 2nd and 3rd quartiles. $n = 15$ (1 wt%) or 12 (1.5, 2 wt%) hydrogels per experimental group. At least 3500 spheroids were analyzed per experimental condition.

When normalized to hydrogel volume to consider differences in swelling, average spheroid volumes of 1 wt% and 1.5 wt% NorHA hydrogels were equivalent **(Figure S2)**. It was found that both hydrogel weight percentage and day of culture influenced the normalized average spheroid volume with spheroids in 1 wt% and 1.5 wt% hydrogels showing significantly higher levels than spheroids in 2 wt% hydrogels ($\alpha < 0.05$). Normalized average spheroid volume was also significantly increased for all groups at days 3 and 7 compared to day 1 ($\alpha < 0.05$). We hypothesized that our hydrogel groups could support different numbers of spheroids, which would change the total spheroid volume compared to average spheroid measurements. The time of culture affected the total spheroid volume with significantly higher levels quantified at day 7 compared to day 1 ($\alpha < 0.05$) (**Figure S3**).

We next quantified OPC viability by measuring the total live spheroid volume to dead spheroid volume ratio (**Figure 5**). This measurement is consistent with viability data (Figure 3) and spheroid volume (Figure 4), where the 1wt% condition results in the greatest survival and growth. Egawa et al. reported viability of OPCs in collagen/hyaluronan hydrogels, supported in part through lactate dehydrogenase (LDH) release, with values peaking at around 75%.[49] In our NorHA hydrogels we used the total live to dead volume ratio to report viability with ratios of 6.7, 4.2, and 2.1 quantified at day 7 for the 1, 1.5, and 2 wt% hydrogel groups respectively. These ratios correspond to 87%, 81%, and 73% viability for the 1, 1.5, and 2 wt% hydrogel groups respectively. Crosslinked GMHA hydrogels showed maximum human aortic endothelial cell viability of ~ 90%

which is comparable to our work. Therefore cell viability remains high when mesh size decreases by an order of magnitude from GMHA hydrogels to NorHA hydrogels.

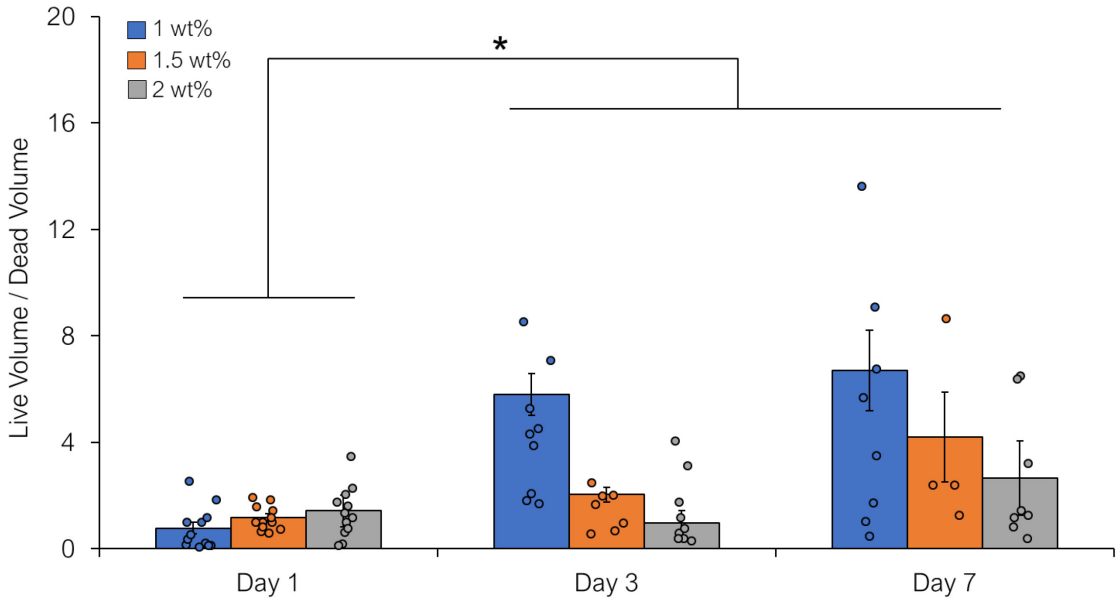

Figure 5: OPC live/dead volume ratio. The ratio of total live spheroid volume to dead spheroid volume was calculated for all experimental groups with 1 wt% hydrogels supporting higher live volume ratios compared to other groups at days 3 and 7 ($\alpha < 0.05$). For each experimental group, bar height represents the average live/dead volume ratio, circles represent individual data points, and error bars represent the standard error of the mean. * indicates a statistically significant difference between day 1 compared to days 3 and 7 ($\alpha < 0.05$). $n = 4$-13 hydrogels per experimental group.

After measuring OPC viability and spheroid formulation, we next sought to track OPC metabolic health in HA hydrogels over a 7 day culture period. We first measured OPC mitochondrial metabolic activity by measuring AlamarBlue reduction (**Figure 6**). This assay can be used to assess OPC metabolic activity in hydrogel samples over an extended period of time in a non-destructive manner by introducing a resazurin dye that is reduced to the fluorescent byproduct resorufin in the electron transport chain without interfering with it.[50] The dye is reduced before oxidative phosphorylation, and requires $2H^+$ and $2e^-$ from the Krebs cycle per molecule to be reduced. We found that metabolic activity levels were similar amongst hydrogel groups at each

time point with significantly higher values measured at day 7 compared to days 1 and 3 for all groups ($\alpha < 0.05$).

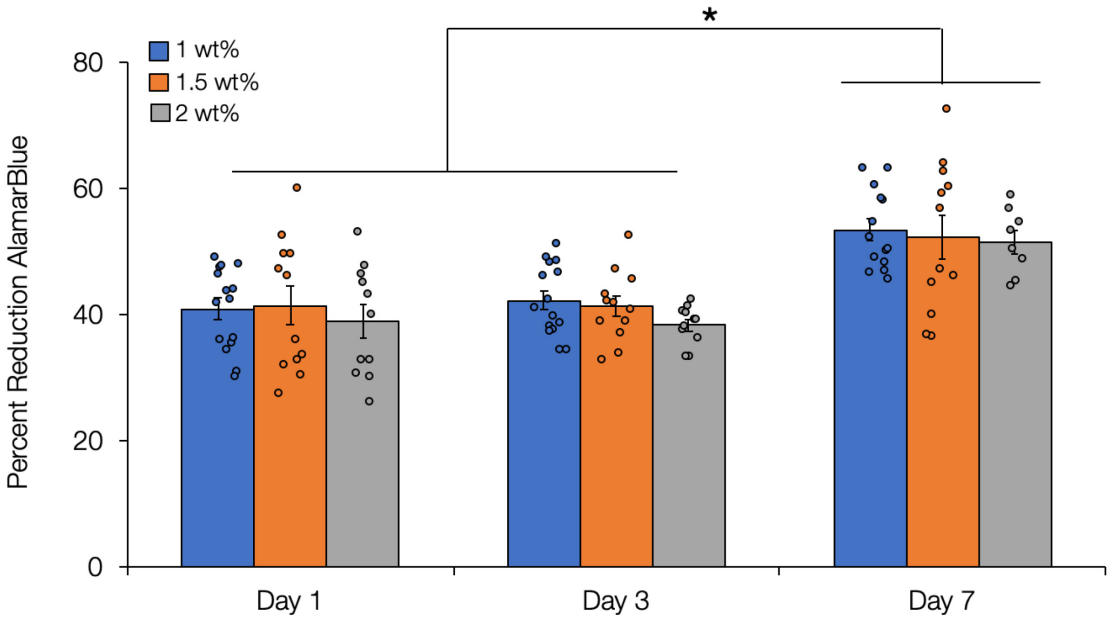

Figure 6: OPC mitochondrial metabolic activity. OPC metabolic activity in HA hydrogels was measured by AlamarBlue reduction. Hydrogels supported similar levels of metabolic activity at each time point with higher values measured at day 7. For each experimental group, bar height represents the average percentage reduction of AlamarBlue, circles represent individual data points, and error bars represent the standard error of the mean. * indicates a statistically significant increase in metabolic activity at day 7 compared to days 1 and 3 ($\alpha < 0.05$). $n = 9$ (1 and 2 wt%) or 12 (1.5 wt%) hydrogels per experimental group.

We also measured OPC DNA concentration in hydrogels and observed similar trends to those found with AlamarBlue metabolic activity measurements with significantly higher DNA levels quantified at day 7 compared to days 1 and 3 for all hydrogel groups (**Figure 7A**). This increase in DNA content indicates that OPCs are undergoing substantial proliferation inside the NorHA hydrogels. These results are comparable to our previous findings with PEGDM hydrogels, where a statistically significant difference in DNA concentration was found between 240 Pa and higher stiffness (560, 1910 Pa) hydrogels.[36]

ATP concentration was also quantified as another measurement of OPC metabolic activity in HA hydrogels. ATP concentrations progressively increased in each hydrogel group as a function of culture time (**Figure 7B**). The lowest stiffness hydrogels demonstrated the highest ATP concentrations with significantly lower ATP levels measured in the stiffest (2 wt%) hydrogels at day 7. This corroborates our previous work with PEGDM hydrogels where the stiffer hydrogels showed lower ATP activity.[36] After normalization of ATP to DNA levels as a measure of average metabolic activity per cell (**Figure 7C**), it was found that the day of culture had a significant influence with higher levels observed at day 7 compared to day 1 for all hydrogel groups. Additionally a trend toward higher ATP per DNA for lower stiffness hydrogels was observed at day 7.

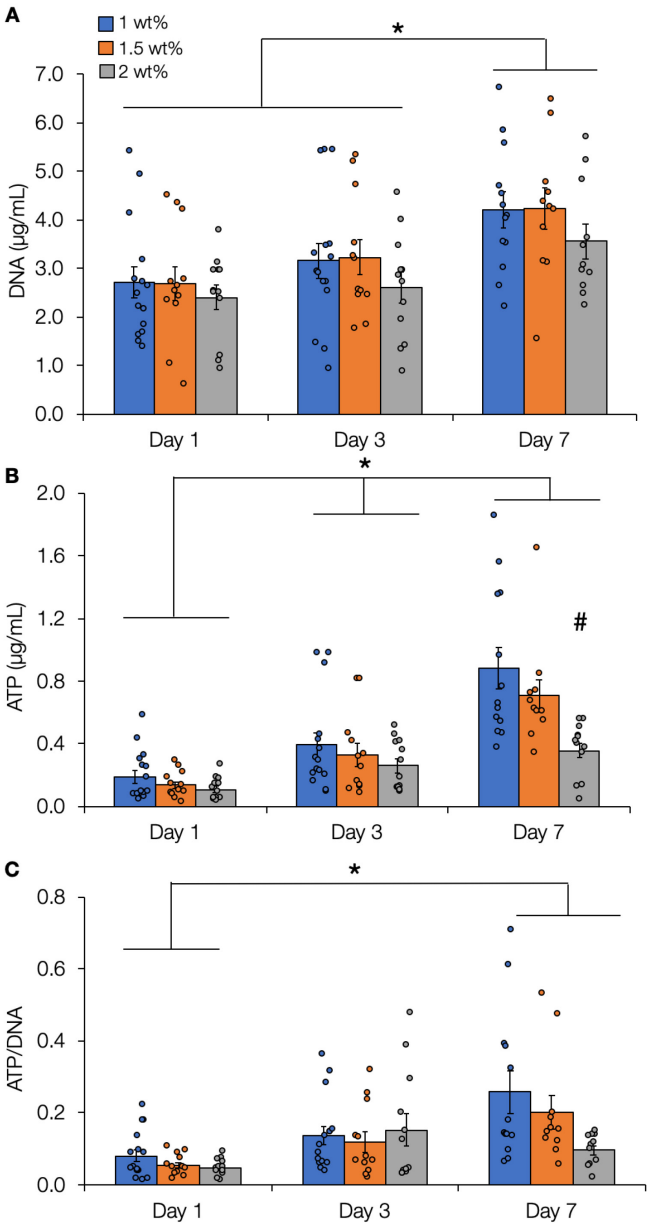

Figure 7: OPC ATP and DNA levels. (A) OPCs encapsulated in 1, 1.5, or 2 wt% NorHA hydrogels all proliferated over a period of 7 days. (B) OPCs also showed progressively increasing ATP concentration over a period of 7 days for all hydrogel groups. (C) Normalizing ATP to DNA concentrations demonstrated higher metabolic activity per cell at day 7 for all hydrogel groups with a trend toward increasing levels for OPCs in lower stiffness hydrogels. For each experimental group, bar height represents the average value for the data set, circles represent individual data points, and error bars represent the standard error of the mean. * indicates statistically significant differences between time points ($\alpha < 0.05$), # indicates statistically significant differences between the 2 wt% and other hydrogel groups at a specific time point. n = 11-15 hydrogels per experimental group.

The two cell metabolic activity assays performed (AlamarBlue, Cell Glo) offer an interesting point of comparison in our assessment of overall OPC health in HA hydrogels. The Cell Glo assay only monitors ATP production, including the 2 molecules of ATP produced by glycolysis and 30 molecules produced through oxidative phosphorylation per glucose molecule in cellular respiration.[51] In contrast, the AlamarBlue assay measures NADH-dependent enzymatic reduction of resazurin to the fluorescent byproduct resorufin which has a considerably smaller scale of measurable output per cycle. The contrast in production scale between these assays suggests that Cell Glo may highlight sharper, more specific differences in energy metabolism between OPCs in different hydrogels, which is indeed what we observed (**Figure 6, 7)**.

Although our ATP/DNA results suggest that there is an inverse relationship between metabolic activity per cell and hydrogel stiffness, this relationship is non-linear. We also observe a non-linear relationship between hydrogel stiffness and mesh size. A 4.6-fold increase in stiffness (1.5 wt% in comparison to 1 wt%) corresponds to a ~ 11.6% reduction in mesh size (**Table 1**). A 12-fold increase in stiffness (2 wt% in comparison to 1 wt%) corresponds to a ~ 14.5% decrease in mesh size (**Table 1**). This is similar to our previous work with PEGDM hydrogels where a 2.6-fold increase in stiffness led to a mesh size change from 9.47 nm to 6.61 nm (30% decrease) as well as significant decreases in ATP concentration.[36] The evidence from this study and our previous work suggests that OPC metabolic activity per cell is affected by the non-linear relationship between hydrogel stiffness and mesh size. Viability is similar across experimental groups (73-87%). In taking a closer look, the peak in total spheroid volume per hydrogel volume on day 3 for 1 wt% hydrogels (Figure S3) may indicate the presence of competing forces. We would expect the number of spheroids to be inversely correlated with the spheroid volume under similar proliferation rates across experimental groups. Since the normalized average spheroid

volume and proliferation is similar on day 7 between 1 wt% and 1.5 wt%, we conclude that the 1 wt% experimental group consists mostly of a small number of large clusters in comparison to a large number of smaller clusters in the 1.5 wt% hydrogels. This is reflected in average spheroid size (Figure 4). Similar normalized average spheroid volumes between 1 wt% and 1.5 wt% hydrogels on day 7 (Figure S2) indicate sparsity of large cell clusters in 1 wt% hydrogels in comparison to denser packing of smaller cell clusters in the 1.5 wt% hydrogels.

Considering the hydrodynamic radii of most proteins is on the order of 1-6 nm,[52] all hydrogels could likely support adequate diffusion of necessary biomolecules. Interestingly, 1.5 wt% and 2 wt% hydrogels supported similar average OPC spheroid volumes (**Figure 4**). ~~despite reduced metabolic activity per cell measurements in 2 wt% hydrogels. However normalizing the average spheroid volumes to the hydrogel volume (Figure S2) leads~~ The proliferation of 1.5 wt% hydrogels and 2 wt% hydrogels are slightly different on day 7. When examining normalized average spheroid volume (Figure S2), the 2 wt% condition lags significantly on day 7 which indicates that the decreased proliferation is magnified by the sparse distribution of cells throughout the volume of the hydrogel despite 1.5 wt% and 2 wt% hydrogels having similar sized cells. In comparison, the cells are more densely packed in the 1.5 wt% hydrogels on day 7.

Normalizing the average spheroid volumes to the hydrogel volume (**Figure S2**) leads to trends that correlate more closely to metabolic activity results (larger spheroids correlate to higher levels of metabolic activity), suggesting that quantification of spheroid volumes in a way that accounts for differences in hydrogel swelling helps explain our metabolic activity results. These results provide an important point of comparison for material systems and strongly indicate that stiffness should not be the sole criteria of interest in 3D mechanobiological studies, at least for OPCs. The OPCs used here capture many characteristics of native cells, but include a p57

knockout, inhibiting their ability to differentiate. It should also be noted that the material system explored here does not give rise to substantial remodeling in the 7 day time course of our experimental study, whereas remodeling may be an important component in both maintenance[53] and differentiation[54] of neural lineages. Despite this, these results may be a good starting place for OPC culture when researchers desire to drive OPC differentiate into oligodendrocytes within a 3D environment. Regardless, ou results may be of note as a tissue culture model of glioma growth in vitro.

Conclusions:

We successfully synthesized and characterized NorHA hydrogels (1, 1.5, and 2 wt%) with mechanical properties resembling CNS tissue (storage moduli of ~ 170, 790, and 2180 Pa respectively). Encapsulated OPCs showed good viability in all HA hydrogel formulations over 7 days of culture. OPCs formed progressively larger spheroids over the culture time with the largest spheroids formed in the lower stiffness (1 wt%) hydrogels with the largest mesh sizes. Average live spheroid volumes were greater than those previously observed in PEGDM hydrogels, perhaps due to larger mesh sizes in the HA hydrogels. Finally, we showed that HA hydrogels supported progressively increasing metabolic activity levels as measured by both AlamarBlue (mitochondrial metabolic activity) and Cell Glo (ATP) assays where ATP levels normalized to DNA were higher in more compliant HA hydrogels. Our results suggest that 3D HA hydrogels could be useful for the growth and expansion of OPCs, and that improved OPC metabolic health is favored in more compliant, larger mesh size, hydrogels.

Supplementary Information:

Supplemental information for this work consists of:

- **(Equations S1 – S4)** – additional equations for determining crosslinking density and mesh size
- **(Figure S1)** – ^{1}H NMR spectrum for NorHA
- **(Table S1)** – Swelling ratios for NorHA hydrogels
- **(Figure S2)** – Average OPC spheroid volume normalized to hydrogel volume
- **(Figure S3)** – Total OPC spheroid volume normalized to hydrogel volume

For Table of Contents Use Only:

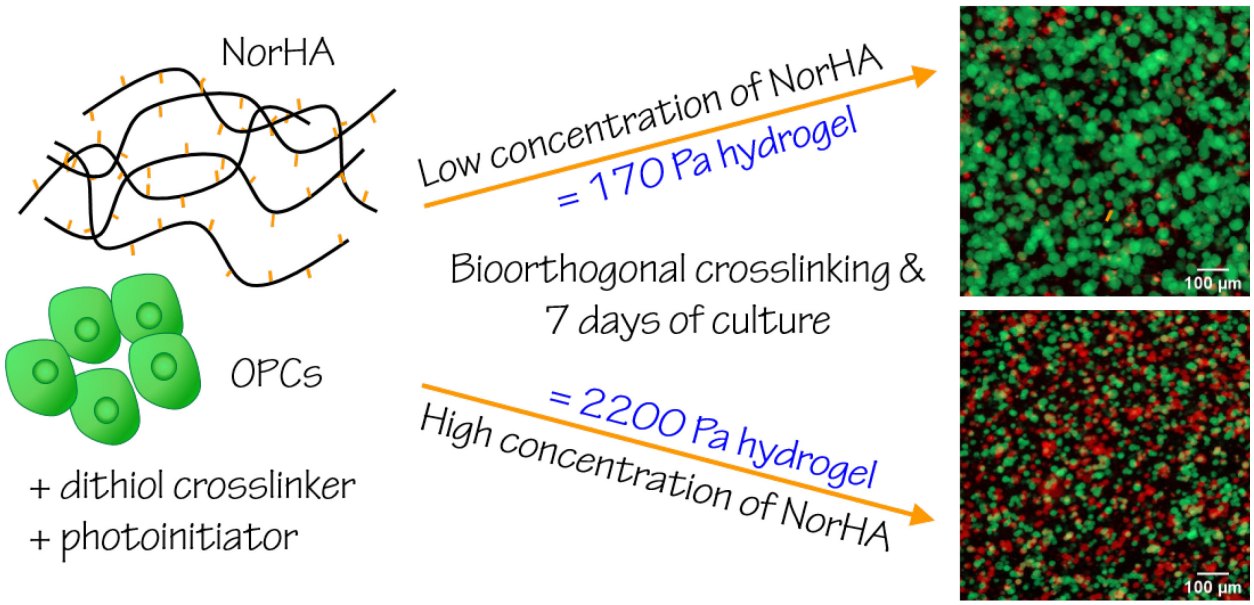

Acknowledgments:

We gratefully acknowledge financial support from NSF grant 1904198 and the Translational Health Research Institute of Virginia for a career development award to KJL. We also acknowledge the Keck Center for Cellular Imaging at the University of Virginia for the usage of the Zeiss 510 microscopy system, NIH grant S10 RR021202 01. Finally we would like to thank the University of Virginia for awarding the Fogg Fellowship (DBU).

References:

1. Popescu, B.F.Gh.; Luchinetti, C.F. Pathology of demyelinating diseases. *Annu. Rev. Pathol.: Mech. Dis.* **2012**, *7,* 185-217.
2. Franklin, R.J.M. Remyelination in the CNS: from biology to therapy. *Nat. Rev. Neuroscience* **2008**, *9*, 839–855.
3. Unal, D.B.; Caliari, S.R.; Lampe, K. J. Engineering biomaterial microenvironments to promote myelination in the central nervous system. *Brain Res. Bull.* **2019,** *152,* 159-174.
4. Purves, D.; Augustine, G.J.; Fitzpatrick, D.; Hall, W.C.; LaMantia, A-S.; Mooney, R.D.; Platt, M.L.; White, L. E. *Neuroscience, Sixth Edition*; Oxford University Press; **2018**.
5. Kandel, E. R., Schwarts, James, H., Jessell, T. M., Siegelbaum, S. A. & Hudspeth, A. J. *Principles Of Neural Science*; McGraw-Hill Education; **2013**. doi:10.1036/0838577016.
6. Hinks, G.L.; Franklin, R.J.M. Distinctive patterns of PDGF-A, FGF-2, IGF-I, and TGF-beta1 gene expression during remyelination of experimentally-induced spinal cord demyelination. *Mol. Cell. Neurosci.* **1999**, *14*, 153–68.
7. Arnett, H.A.; Mason, J.; Marino, M.; Suzuki, K.; Matsushima, G.K.; Ting, J.P. TNF alpha promotes proliferation of oligodendrocyte progenitors and remyelination. *Nat. Neurosci.* **2001**, *4*, 1116–22.
8. Mason, J.L.; Suzuki, K.; Chaplin, D.D.; Matsushima, G.K. Interleukin-1beta promotes repair of the CNS. *J. Neurosci.* **2001**, *21*, 7046–52.
9. Kotter, M.R.; Zhao, C.; Van Rooijen, N.; Franklin, R.J.M. Macrophage-depletion induced impairment of experimental CNS remyelination is associated with a reduced oligodendrocyte progenitor cell response and altered growth factor expression. *Neurobiol. Dis.* **2005**, *18*(1), 166–175.
10. Foote, A.K.; Blakemore, W.F.; Inflammation stimulates remyelination in areas of chronic demyelination. *Brain* **2005,** *128*(3), 528–39.

11. Windrem, M.S.; Nunes, M.C.; Rashbaum, W.K.; Schwartz, T.H.; Goodman, R.A.; McKhann, G.; Roy, N.S.; Goldman, S.A. Fetal and adult human oligodendrocyte progenitor cell isolates myelinate the congenitally dysmyelinated brain. *Nat. Med.* **2004**, *10*(1), 93–97.
12. Manley, N.C.; Priest, C.A.; Denham, J.; Wirth III, E.D.; Lebkowski, J.S. Human embryonic stem cell-derived oligodendrocyte progenitor cells: preclinical efficacy and safety in cervical spinal cord injury. *Stem Cells Transl. Med.* **2017**, *6*(10), 1917–1929.
13. Sharp, J.; Frame, J.; Siegenthaler, M.; Nistor, G.; Keirstead, H.S. Human embryonic stem cell-derived oligodendrocyte progenitor cell transplants improve recovery after cervical spinal cord injury. *Stem Cells* **2010**, *28*(1), 152–163.
14. Keirstead, H.S.; Nistor, G.; Bernal, G.; Totoiu, M.; Cloutier, F.; Sharp, K.; Steward, O. Human embryonic stem cell-derived oligodendrocyte progenitor cell transplants remyelinate and restore locomotion after spinal cord injury. *J. Neurosci.* **2005**, *25*(19), 4694–4705.
15. Priest, C.A.; Manley, N.C.; Denham, J.; Wirth III, E.D.; Lebkowski, J.S. Preclinical safety of human embryonic stem cell-derived oligodendrocyte progenitors supporting clinical trials in spinal cord injury. *Regener. Med.* **2015**, *10*(8), 939–958.
16. Lineage Cell Therapeutics, Inc. *Does escalation study of AST-OPC1 in spinal cord injury*. (2020).
17. Zhu, J.; Marchant, R. E. Design properties of hydrogel tissue-engineering scaffolds. *Expert Rev. Med. Devices* **2011**, *8*(5), 607–626.
18. Tibbitt, M.W.; Anseth, K. S. Hydrogels as extracellular matrix mimics for 3D cell culture. *Biotechnol. Bioeng.* **2009**, *103*, 655–663.
19. Caliari, S.R.; Burdick, J. A. A practical guide to hydrogels for cell culture. *Nat. Methods* **2016**, *13*(5), 405.
20. Lampe, K.J.; Mooney, R.G.; Bjugstad, K.B.; Mahoney, M. J. Effect of macromer weight percent on neural cell growth in 2D and 3D nondegradable PEG hydrogel culture. *J. Biomed. Mater. Res., Part A* **2010**, *94*(4), 1162–1171.
21. Asmani, M. N., Ai, J., Amoabediny, G. & Noroozi, A. Three-dimensional culture of differentiated endometrial stromal cells to oligodendrocyte progenitor cells (OPCs) in fibrin hydrogel. *Cell Biol. Int.* **2013**, *37*(12), 1340–1349. https://doi.org/10.1002/cbin.10171.
22. Tabesh, H.; Amoabediny, G.H.; Nik, N.S.; Heydari, M.; Yoesfifard, M.; Siadat, S.R.; Mottaghy, K. The role of biodegradable engineered scaffolds seeded with Schwann cells for spinal cord regeneration. *Neurochem. Int.* **2009**, *54*(2), 73–83.
23. Highley, C.B.; Prestwich, G.D.; Burdick, J. A. Recent advances in hyaluronic acid hydrogels for biomedical applications. *Curr. Opin. Biotechnol.* **2016**, *40*, 35–40.
24. Seidlits, S.K.; Liang, J.; Bierman, R.D.; Sohrabi, A.; Karam, J.; Holley, S.M.; Cepeda, C.; Walthers, C. M. Peptide-modified, hyaluronic acid-based hydrogels as a 3D culture platform for neural stem / progenitor cell engineering. *J. Biomed. Mater. Res., Part A* **2019**, *107*(4), 704–718.
25. Back, S.A.; Tuohy, T.M.; Chen, H.; Wallingford, N.; Craig, A.; Struve, J.; Luo, N. L. Hyaluronan accumulates in demyelinated lesions and inhibits oligodendrocyte progenitor maturation. *Nat. Med.* **2005**, *11*(9), 966.
26. Preston, M.; Gong, X.; Su, W.; Matsumoto, S.G.; Banine, F.; Winkler, C.; Foster, S. Digestion products of the PH20 hyaluronidase inhibit remyelination. *Ann. Neurol.* **2013**, *73*(2), 266–280.
27. Khaing, Z. Z. & Seidlits, S. K. Hyaluronic acid and neural stem cells: implications for biomaterial design. *J. Mater. Chem. B* **2015**, *3*(40), 7850–7866. https://doi.org/10.1039/C5TB00974J.
28. Isa, I.L.; Srivastava, A.; Tiernan, D.; Owens, P.; Rooney, P.; Dockery, P.; Pandit, A. Hyaluronic acid based hydrogels attenuate inflammatory receptors and neurotrophins in interleukin-1B induced inflammation model of nucleus pulposus cells. *Biomacromolecules* **2015**, *16*(6), 1714–1725.
29. Li, X.; Liu, X.; Cui, L.; Brunson, C.; Zhao, W.; Bhat, N.R.; Zhang, N.; Wen, X. Engineering an in situ crosslinkable hydrogel for enhanced remyelination. *FASEB J.* **2013**, *27*(3), 1127–1136.

30. Seidlits, S.K.; Khaing, Z.Z.; Petersen, R.R.; Nickels, J.D.; Vanscoy, J.E.; Shear, J.B.; Schmidt. The effects of hyaluronic acid hydrogels with tunable mechanical properties on neural progenitor cell differentiation. *Biomaterials* **2010**, *31*(14), 3930-3940.
31. Back, S.A.; Tuohy, T.M.; Chen, H.; Wallingford, N.; Craig, A.; Struve, J.; Luo, N. L. Hyaluronan accumulates in demyelinated lesions and inhibits oligodendrocyte progenitor maturation. *Nat. Med.* **2005**, *11*(9), 966.
32. Russell, L.N.; Lampe, K. J. Engineering biomaterials to influence oligodendroglial growth, maturation, and myelin production. *Cells Tissues Organs* **2016**, *202*(1-2), 85–101.
33. Segel, M.; Neumann, B.; Hill, M.F.; Weber, I.P.; Viscomi, C.; Zhao, C.; Young, A.; Agley, C.C.; Thompson, A.J.; Gonzalez, G.A.; Sharma, A. Niche stiffness underlies the ageing of central nervous system progenitor cells. *Nature* **2019**, *573*(7772) , 130–134.
34. Pu, A.; Stephenson, E.L.; Yong, V. W. The extracellular matrix: Focus on oligodendrocyte biology and targeting CSPGs for remyelination therapies. *Glia* **2018**, *66*(9), 1809–1825.
35. Jagielska, A.; Norman, A.L; Whyte, G.; Van Vilet, K.J.; Guck. J.; Franklin, R. J. M. Mechanical environment modulates biological properties of oligodendrocyte progenitor cells. *Stem Cells Dev.* **2012**, *21*(16), 2905–2914.
36. Russell, L. N.; Lampe, K. J. Oligodendrocyte precursor cell viability, proliferation, and morphology is dependent on mesh size and storage modulus in 3D poly(ethylene glycol)-based hydrogels. *ACS Biomater. Sci. Eng.* **2017**, *3*(12), 3459–3468. https://doi.org/10.1021/acsbiomaterials.7b00374
37. Fallacara, A.; Baldini, E.; Manfredini, S.; Vertuani, S. Hyaluronic acid in the third millennium. *Polymers* **2018**, 10, 701.
38. Liu, C.; Sage, J.C.; Miller, M.R.; Verhaak, R.G.; Hippenmeyer, S.; Vogel, H.; Foreman, O.; Bronson, R.T.; Nishiyama, A.; Luo, L.; Zong, H. Mosaic analysis with double markers reveals tumor cell of origin in glioma. *Cell* **2011**, 146, 209–221.
39. Takahashi, K.; Yamanaka, S. Induction of pluripotent stem cells from mouse embryonic and adult fibroblast cultures by defined factors. *Cell* **2006**, 126, 663–676.
40. Gramlich, W.M.; Kim, I.L; Burdick, J. A. Synthesis and orthogonal photopatterning of hyaluronic acid hydrogels with thiol-norbornene chemistry. *Biomaterials* **2013**, *34*(38), 9803–9811.
41. Widjaja, L.K.; Bora, M.; Chan, P.N.P.H.; Lipik, V.; Wong, T.T.; Venkatraman, S. S. Hyaluronic acid-based nanocomposite hydrogels for ocular drug delivery applications. *J. Biomed. Mater. Res., Part A* **2014**, *102*(9), 3056–3065.
42. Yang, T. Mechanical and swelling properties of hydrogels. Diss. KTH Royal Institute of Technology, **2012**.
43. Leach, J.B.; Bivens, K.A.; Patrick, C.W.; Schmidt, C. E. Photocrosslinked hyaluronic acid hydrogels: natural, biodegradable tissue engineering scaffolds. *Biotechnol. Bioeng.* **2003**, *82*(5), 578–589.
44. Caliari, S.R.; Vega, S.L.; Kwon, M.; Soulas, E.M.; Burdick, J. A. Dimensionality and spreading influence MSC YAP/TAZ signaling in hydrogel environments. *Biomaterials* **2016**, *103*, 314–323.
45. Ingber, D. Mechanobiology and diseases of mechanotransduction. *Ann. Med.* **2003**, *35*(8), 564–577.
46. Li, X., Katsanevakis, E., Liu, X., Zhang, N. & Wen, X. Engineering neural stem cell fates with hydrogel design for central nervous system regeneration. *Prog. Polym. Sci.* **2012**, *37*(8), 1105–1129. https://doi.org/10.1016/j.progpolymsci.2012.02.004.
47. Li, X.; Liu, X.; Cui, L.; Brunson, C.; Zhao, W.; Bhat, N.R.; Zhang, N.; Wen, X. Engineering an in situ crosslinkable hydrogel for enhanced remyelination. *FASEB J.* **2013**, *27*(3), 1127–1136.
48. Kwon, M.Y.; Wang, C.; Galarraga, J.H.; Pure, E.; Han, L.; Burdick, J.A. Influence of hyaluronic acid modification on CD44 binding towards the design of hydrogel biomaterials. *Biomaterials* **2019**, 222, 119451.

49. Egawa, N.; Shindo, A.; Liang, A.C.; Du, Y.; Xing, C.; Lo, E.K.; Itoh, K.; Konshita, H.; Maki, T.; Takahashi, R.; Sudo, R.A. A novel three-dimensional culture system for oligodendrocyte precursor cells. *Stem Cells Dev.* **2017**, *26*(14), 1078–1085. https://doi.org/10.1089/scd.2016.0306.
50. Rampersad, S. N. Multiple applications of Alamar Blue as an indicator of metabolic function and cellular health in cell viability bioassays. *Sensors* **2012**, *12*(9), 12347–12360.
51. Alberts, B.; Johnson, A.; Lewis, J.; Raff, M.; Roberts, K.; Walter, P. *Molecular Biology of the Cell, 5th ed.;* Garland Science; **2008**.
52. Erickson, H. P. Size and shape of protein molecules at the nanometer level determined by sedimentation, gel filtration, and electron microscopy. *Biological Proced. Online* **2009**, *11*(1), 32.
53. Madl, C.M.; LeSavage, B.L.; Dewi, R.E.; Dinh, C.B.; Stowers, R.S.; Khariton, M.; Lampe, K.J.; Nguyen, D.; Chaudhuri, O.; Enejder, A.; Heilshorn, S. C. Maintenance of neural progenitor cell stemness in 3D hydrogels requires matrix remodeling. *Nat. Mater.* **2017**, *16*(12), 1233–1242.
54. Madl, C.M.; LeSavage, B.L.; Dewi, R.E.; Lampe, K.J.; Heilshorn, S. C. Matrix remodeling enhances the differentiation capacity of neural progenitor cells in 3D hydrogels. *Adv. Sci.* **2019**, *6*(4), 1801716.